NASA TECHNICAL NOTE

NASA TN D-2397

NASA TN D-2397

RADIATIVE EQUILIBRIUM IN PLANETARY ATMOSPHERES.

I. APPLICATION OF THE STRONG LINE ABSORPTION LAW TO THE ATMOSPHERE OF VENUS

by Rudolf A. Hanel and Frank Bartko

Goddard Space Flight Center

Greenbelt, Md.

NATIONAL AERONAUTICS AND SPACE ADMINISTRATION • WASHINGTON, D. C. • AUGUST 1964

RADIATIVE EQUILIBRIUM IN PLANETARY ATMOSPHERES. I. APPLICATION OF THE STRONG LINE ABSORPTION LAW TO THE ATMOSPHERE OF VENUS

By Rudolf A. Hanel and Frank Bartko

Goddard Space Flight Center
Greenbelt, Md.

NATIONAL AERONAUTICS AND SPACE ADMINISTRATION

For sale by the Office of Technical Services, Department of Commerce,
Washington, D.C. 20230 -- Price $0.75

RADIATIVE EQUILIBRIUM IN PLANETARY ATMOSPHERES. I. APPLICATION OF THE STRONG LINE ABSORPTION LAW TO THE ATMOSPHERE OF VENUS

by
Rudolf A. Hanel and Frank Bartko
Goddard Space Flight Center

SUMMARY

The interpretation of the data obtained for Venus in the 8-12μ atmospheric window clearly requires some knowledge of the temperature distribution in the planet's upper atmosphere. For this purpose temperatures, net fluxes, and specific intensities were calculated for a CO_2-N_2 atmosphere in radiative equilibrium. The wavelength, temperature, and pressure dependence of the CO_2 absorption, including the excited bands, was considered. Solar radiation absorbed in the clear atmosphere influences the temperature profile distinctly. The effects of various CO_2 concentrations, cloud top pressure levels, and cloud reflectivities on the equilibrium temperatures are also discussed.

CONTENTS

List of Symbols

$\bar{A}_i$	– Fractional absorptance in the wavelength interval i.
$B_\nu(T)$	– Planck function at temperature T (watts cm^{-2} $ster^{-1}$ wave $number^{-1}$).
c	– Subscript denoting cloud surface.
$E_n(\tau)$	– Exponential integral of order n.
$\pi F_\nu(\tau_\nu)$	– Spectral total flux at τ_ν (watts cm^{-2} wave $number^{-1}$).
H	– Pressure scale height (H_0 = value at 273°K).
i	– Index denoting wave number interval.
$I_\nu(\mu, \tau_\nu)$	– Specific intensity (watts cm^{-2} $ster^{-1}$ wave $number^{-1}$).
j	– Index denoting vertical coordinate.
$J_\nu(\tau_\nu)$	– Spectral mean intensity at optical depth τ_ν (watts cm^{-2} wave $number^{-1}$ $ster^{-1}$).
l_ν	– Generalized absorption coefficient, $l = m^n$ (cm^{-1} NTP).
m	– Parameter defined in Equation 19.
n	– Exponent defined in Equations 2 and 19.
P	– Pressure (P_0 = 1 atm).
q	– CO_2 volume concentration.
r_{ic}	– Cloud reflectivity in wave number interval i.
s	– Geometric path length (cm).
S_ν	– Solar constant in wave number interval 18 (watts cm^{-2}).
t	– Integration variable.
T	– Atmospheric temperature (T_0 = 273°K).
u	– Path length of active gas at NTP (cm).
u*	– Modified pressure- and temperature-reduced path length (cm). See Equation 16.
X	Parameter proportional to the product of the spectral line intensity and the ratio of path length to line half width.
α	-- Flux convergence criterion (Equation 40).
β	– Parameter proportional to the ratio of the spectral line half-width to the average line spacing.
γ	– Exponent describing the temperature dependence of excited bands (Equation 13).

$\epsilon_{\nu c}$ – Spectral emissivity of cloud surface.

ζ – Cosine of the solar zenith angle.

μ – Direction cosine ($\mu = \cos\theta$).

ν – Wave number (cm^{-1}).

ρ – Atmospheric density.

$\tau_{\mu\nu}$ – Optical thickness in direction μ at wave number ν.

ω – Solid angle (ster).

RADIATIVE EQUILIBRIUM IN PLANETARY ATMOSPHERES. I. APPLICATION OF THE STRONG LINE ABSORPTION LAW TO THE ATMOSPHERE OF VENUS*

by
Rudolf A. Hanel and Frank Bartko
Goddard Space Flight Center

INTRODUCTION

The structure of a planet's atmosphere is governed primarily by convective and radiative energy transport. On the earth, convective processes preponderate in the troposphere and radiative processes in the stratosphere. Similarly, the atmospheres of Mars and Venus should exhibit zones of convective and radiative transfer. Convection probably characterizes the Venus atmosphere below the cloud level, especially if the clouds consist of dust particles, whereas the region above the cloud layer is probably dominated by radiative transfer. The interpretation of infrared measurements of the atmospheres of the terrestrial planets must, therefore, be based on the theory of radiative transfer and appropriately modified for convection where necessary. The objectives of the program discussed in this paper were to establish an analytical tool for the study of planetary atmospheres based on the radiative transfer theory. An initial version of this program has been applied to the atmosphere of Venus. This application must be used with relatively inaccurate estimates of physical parameters which influence the solution of the transfer equation. However, the program permits a parametric study where the number of possible solutions is ultimately restricted by observational constraints.

The equilibrium temperature distribution of an N_2-CO_2 atmosphere was calculated for several volume concentrations of CO_2. The wavelength, temperature, and pressure dependence of the absorption coefficients was taken into account. The effect of direct and diffusely reflected solar radiation absorbed by the atmosphere was also included. An effective surface emissivity was introduced as an additional parameter and permitted a deviation from the usual assumption that the surface radiates like a blackbody in the infrared. In addition to the radiative equilibrium temperatures, the specific intensities were calculated. Net fluxes were obtained by angular integration, taking into account fully the dependence of the intensity on direction. The simplifying procedure of converting parallel beam radiation to an equivalent diffuse radiation field was avoided (References 1-3).

*This report was presented at the Conference on Atmospheric Radiation, Eppley Laboratories, Newport, Rhode Island, and will be published in an American Meteorological Society Monograph.

The net flux of a planet can be determined independently from the heat budget by considering the observed albedo and the appropriate value of the solar constant. This restricts the number of theoretically possible solutions, since only those which yield total flux values consistent with the albedo can be admitted. The number of solutions can be restricted further by a comparison of calculated and measured values of the specific intensity at several wavelength intervals and zenith angles.

In the discussion below, the assumptions and limitations of the calculations are stated and the mathematical formulation is presented. An illustration of the effects of the various parameters on the temperature profiles follows, but further conclusions will be discussed elsewhere.

SOLUTION OF THE RADIATIVE TRANSFER EQUATION

In order to calculate the equilibrium temperatures in a finite, nongrey, optically thick atmosphere, the equation of radiative transfer must be solved, subject to appropriate boundary conditions (Reference 4, for example). The assumption of radiative equilibrium holds as long as the atmosphere is stable against convection (Reference 5, for example). Stability, in turn, is maintained as long as the temperature gradient is everywhere less than the adiabatic gradient.

For the particular application considered here, the surface is taken to be the cloud tops and is assumed to be the demarcation between regions of energy transport dominated by radiation and convection. It is realized that the assumption of a solid surface for the clouds is a severe simplification. A more rigorous treatment would apply the theory of radiative transfer for a scattering medium (Reference 6, for example).

For an atmosphere in local thermodynamic equilibrium the equation of transfer is

$$\frac{dI_\nu(\mu, \tau_{\mu\nu})}{d\tau_{\mu\nu}} = I_\nu(\mu, \tau_{\mu\nu}) - B_\nu(T) , \tag{1}$$

where $B_\nu(T)$ is the Planck function and $I_\nu(\mu, \tau_{\mu\nu})$ the specific intensity of the radiation field. For radiative transfer calculations dealing with strong molecular band absorption, the optical thickness $\tau_{\mu\nu}$ can be expressed

$$\tau_{\mu\nu}(l_\nu, u^*, \mu) = l_\nu \left(\frac{u^*}{\mu}\right)^n = \frac{\tau_\nu(l_\nu, u^*)}{\mu^n} , \tag{2}$$

where l_ν is a generalized absorption coefficient and u^*/μ a pressure- and temperature-reduced path length. It is convenient to use the optical path in the vertical direction, τ_ν, and the direction cosine μ, instead of the optical path, $\tau_{\mu\nu}$, in an arbitrary direction. The appearance of μ under the exponent n has a significant influence on the transfer problem. The value of n is unity for weak line or grey absorption and one-half or less for the square root or strong line absorption law (Reference 7). In contrast to weak line or grey absorption, the strong line absorption law reduces

the thermal coupling between adjacent atmospheric layers and permits a more effective exchange of radiative energy over greater optical distances.

Very general boundary conditions have been selected. At some optical depth, $\tau_{\nu c}$, the atmosphere is assumed to be bounded by a perfectly diffuse reflector of effective emissivity $\epsilon_{\nu c}$, related to the surface reflectivity by

$$\epsilon_{\nu c} = 1 - r_{\nu c} \quad . \tag{3}$$

For positive values of μ this assumption requires the solution of Equation 1 at the boundary $\tau_{\nu c}$ to be

$$I_\nu^+(\tau_\nu = \tau_{\nu c}) = \epsilon_{\nu c} B_\nu(T_c) + r_{\nu c} F_\nu^-(\tau_{\nu c}) + \frac{S_\nu}{\pi} \zeta r_{\nu c} e^{-\frac{\tau_{\nu c}}{\zeta^n}} \quad . \tag{4}$$

The first term on the right represents the thermal emission by the surface of temperature T_c. The second term arises from the nonblack characteristic of the surface; the downward flux incident on the surface is partially reflected back into the atmosphere. The third term describes the reflected solar component.

At the top of the atmosphere where $\tau_\nu = 0$ only solar radiation is assumed incident. For thermal radiation outer space is considered a perfect sink. Hence the upper boundary condition is

$$I_\nu^-(\zeta, \tau_\nu = 0) = \frac{S_\nu}{\pi} \zeta \quad . \tag{5}$$

The solution of the transfer equation subject to the boundary conditions and the absorption law for τ_ν may be verified to be

$$I_\nu^+(\mu, \tau_\nu) = \epsilon_{\nu c} B_\nu(T_c) e^{-\frac{\tau_{\nu c} - \tau_\nu}{\mu^n}} + \int_{\tau_\nu}^{\tau_{\nu c}} B_\nu(t) e^{-\frac{t - \tau_\nu}{\mu^n}} \frac{dt}{\mu^n}$$

$$+ r_{\nu c} e^{-\frac{\tau_{\nu c} - \tau_\nu}{\mu^n}} \frac{2}{n} \int_0^{\tau_{\nu c}} B_\nu(t) E_{\frac{2}{n}}(\tau_{\nu c} - t) dt + \frac{S_\nu}{\pi} r_{\nu c} \zeta e^{-\frac{\tau_{\nu c}}{\zeta^n}} e^{-\frac{\tau_{\nu c} - \tau_\nu}{\mu^n}} \quad , \tag{6}$$

and

$$I_\nu^-(\mu, \tau_\nu) = \int_0^{\tau_\nu} B_\nu(t) e^{-\frac{\tau_\nu - t}{\mu^n}} \frac{dt}{\mu^n} + \frac{S_\nu}{\pi} \zeta e^{-\frac{\tau_\nu}{\zeta^n}} \quad . \tag{7}$$

In Equation 6 $I_\nu^+(\mu, \tau_\nu)$ is the upward intensity whose respective components arise from the surface emission, the atmospheric emission by all layers at optical depths greater than τ_ν, and the downward fluxes diffusely reflected upwards. $I_\nu^-(\mu, \tau_\nu)$ is the downward intensity consisting of the atmospheric emission arising from all layers with optical depths less than τ_ν and the incident solar radiation.

The temperature distribution is obtained from a solution of the equation of radiative equilibrium which equates the total emitted and absorbed radiation for each volume element. For a stratified atmosphere each layer must satisfy the energy balance condition

$$\int_\nu \int_\omega \int_V l_\nu \, e^{-\frac{\Delta\tau}{\mu^n}} B_\nu \, dV \, d\omega \, d\nu = \int_\nu \int_\omega \int_V l_\nu \, e^{-\frac{\Delta\tau}{\mu^n}} I_\nu \, dV \, d\omega \, d\nu \quad . \tag{8}$$

The exponential term represents the attenuation losses due to self-absorption in the layer of finite optical thickness. Integration over all directions is required since I_ν as well as $e^{-\Delta\tau/\mu^n}$ is a function of μ. Furthermore, since absorption and emission may occur in different parts of the spectrum the equality holds only if the integration is taken over all frequencies. This general form of the condition of radiative equilibrium applies to any volume element as well as to different forms of absorption laws. If $\Delta\tau$ is very small in all directions, the familiar form (References 8 and 9) of the radiative equilibrium equation results:

$$\int_\nu l_\nu \, B_\nu \, d\nu = \int_\nu l_\nu \, J_\nu \, d\nu \quad . \tag{9}$$

Substitution of the intensities obtained (Equations 6 and 7) into the equation of radiative equilibrium leads to a Milne-type integral equation in $B_\nu(\tau)$, whose solution is required in obtaining the temperature distribution. The solution is obtained by iteration beginning from an assumed temperature distribution. The net flux is computed after each iteration. When the distribution of the net flux is constant within specified limits, radiative equilibrium is achieved and the calculation proceeds to the final step, the computation of limb darkening.

The components of the upward and downward intensities, the net flux, and the condition of radiative equilibrium will be examined in more detail in the manner required for computer solution. Hence a brief description of the coordinate system and the calculation of τ_ν follows.

COORDINATE SYSTEM

A plane parallel atmosphere is assumed and the computations are carried out in a 33 layer coordinate system (Figure 1). The interface between layer $j-1$ and j is called interface j and the quantities u_j^* and τ_j are computed from the top of the atmosphere (interface one, zero pressure) to interface j and the corresponding pressure P_j. In all computations the pressure at

interface j = 2 was taken equal to 10^{-3} atm. Layer one above this level is included for the sake of completeness. The computed temperature is only an average value and it should not be interpreted that layer one is isothermal. For this region of the atmosphere, local thermodynamic equilibrium may not exist (Reference 10, for example) and the absorption law adopted may not strictly apply (Reference 11). In addition, photochemical and other atmospheric processes will have a strong effect on the temperature in this region. For layers between j = 2 and 28, pressures are calculated according to the recursion formula

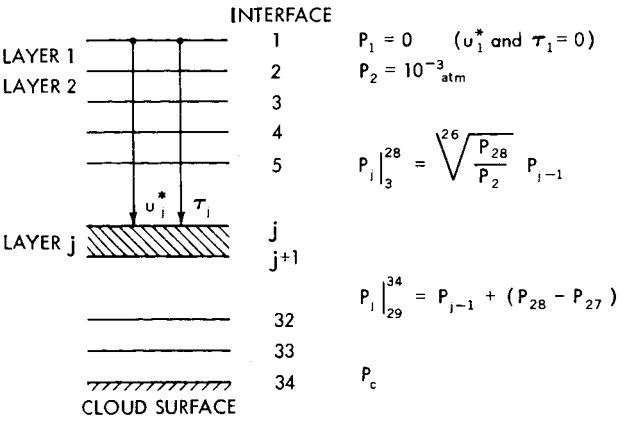

Figure 1—Coordinate system.

$$P_j = \sqrt[26]{\frac{P_{28}}{P_2}}\, P_{j-1} \quad . \tag{10}$$

This mode of pressure slicing yields layers of approximately the same geometrical height but of increasing optical thickness. To avoid a very thick layer adjacent to the cloud boundary, a linear pressure slicing was applied between j = 28 and the surface (j = 34).

ABSORPTION COEFFICIENTS

The calculation of the optical thickness requires a value for the absorption coefficient, which varies with pressure and temperature, and a value for the mass of the absorbing gas. For pressures greater than 10^{-3} atm the individual line shape is determined primarily by collision broadening. The effect of this factor on atmospheric structure has been studied by several authors (Reference 12, for example). For band absorption the concept of optical thickness defined for a single frequency is still very useful, but τ becomes, in general, a complicated function of u^*. For all cases studied in this paper, an analytical expression can be derived for this function, based on the so-called strong line absorption law (Reference 7). This approximation applies to CO_2 within the pressure ranges of interest, namely from 10^{-3} to 1 atm for CO_2 concentrations exceeding 0.01 part per volume.

The mass of active gas is usually expressed in terms of a path length. An element of the path length is defined by the product of the geometric path length ds and the normalized density of the active gas

$$du = q\frac{\rho}{\rho_0}\, ds \quad , \tag{11}$$

Since $\rho = MP/RT$,

$$du = q \frac{P}{P_0} \frac{T_0}{T} ds \quad . \tag{12}$$

In the domain of collision broadening, the pressure and temperature dependences of the half-width of absorption lines are usually considered by defining a reduced path length equal to the product of du, the pressure, and the inverse square root of the temperature. The temperature dependence of the excited bands may be included by an exponential term which represents the increase of the population of the lower vibrational energy state with temperature (Reference 13, for example). An additional temperature dependence of the rotational levels, within each vibrational state, has the effect of altering the band shape. However, this effect is much smaller than that due to changes in the population of the vibrational state. The reduced path length, with these effects, is then

$$du^* = q\left(\frac{P}{P_0}\right)^2 \left(\frac{T_0}{T}\right)^{3/2} e^{\gamma\left(\frac{1}{250} - \frac{1}{T}\right)} ds \quad . \tag{13}$$

The numerical value of γ was computed from Reference 14 for each spectral region, and the adopted values are listed in Table 1. The value μds equals the vertical path element dh. Thus, by using the hydrostatic equation

$$\frac{dh}{H} = - \frac{dP}{P} \quad , \tag{14}$$

the reduced path length in a direction μ can be expressed by

$$du^*(\mu) = - \frac{1}{\mu} qH_0 \left(\frac{T_0}{T}\right)^{1/2} e^{\gamma\left(\frac{1}{250} - \frac{1}{T}\right)} \frac{P\, dP}{P_0^2} \quad . \tag{15}$$

For the remainder of this paper, only the reduced path length in the vertical direction, $u^*(\mu = 1)$, is used. The reduced path length from a level P to outer space is a function of the wavelength as well as the temperature profile,

$$u_\nu^* = qH_0 \int_0^P \left[\frac{T_0}{T(P)}\right]^{1/2} e^{\gamma_\nu \left(\frac{1}{250} - \frac{1}{T(P)}\right)} \frac{P\, dP}{P_0^2} \quad . \tag{16}$$

For the numerical computations Equation 16 was reformulated in terms of the adopted coordinate system,

$$u_{ij}^* = u_{i,j-1}^* + qH_0 \left(\frac{T_0}{T_{j-1}}\right)^{1/2} e^{\gamma_i \left(\frac{1}{250} - \frac{1}{T_{j-1}}\right)} \frac{P_j^2 - P_{j-1}^2}{2P_0^2} \quad . \tag{17}$$

A constant temperature within each layer is assumed. The scale height H_0 for standard

temperature is a function of the molecular weight and, therefore, of the fractional concentration of each gas; adopted values are given in Table 2.

Since CO_2 is the primary absorbing constituent, an accurate representation of its absorption spectrum as a function of pressure, temperature, and path length is required. The absorption spectrum of CO_2 can be separated into three important regions. The near infrared region from 1 to about 6μ is most important in regard to the absorption of solar radiation but less significant in regard to the thermal emission spectrum of the clouds (Reference 15). The 9.4 and 10.4μ excited bands of CO_2 are within the second region considered in this calculation. They lie in a spectral region for which planetary observations exist (References 16-18), although they play only a minor role in the determination of the atmospheric structure. Any realistic interpretation of the data from References 16-18 must necessarily represent this part of the spectrum adequately. The strong bands near 15μ determine the atmospheric structure in the radiative regime; the interval of 12-20μ is the third region considered.

The spectrum should be divided into many intervals for accurate representation, but the number of intervals must be limited to avoid unreasonably long computing times. As a compromise, the 18 intervals listed in Table 1 were selected.

For the pressure and temperature ranges considered, the individual line shapes are controlled primarily by collision broadening. For high concentrations of CO_2 ($q \geq 0.01$) the distribution of the lines and their spacings in the major bands indicates appreciable overlapping. The square root law would overestimate the absorption in such intervals; but the strong line approximation is a generalization of this law which is valid even when overlapping occurs. This approximation is expressed in terms of a single variable u^* and is well suited to extrapolation of the absorption to large path lengths and low pressures (Reference 7).

Table 1

Values used in the Computation of CO_2 Absorption for Various Spectral Intervals.

i	ν (cm^{-1})	m	n	γ
1	0-200	0	0.50	0
2	200-300	0	0.50	0
3	300-400	0	0.50	0
4	400-495	0	0.50	0
5	495-550	7.8×10^{-5}	0.60	0
6	550-625	4.6×10^{-3}	0.42	0
7	625-660	9.0×10^{-1}	0.38	0
8	660-720	4.9×10^{-1}	0.42	0
9	720-810	9.5×10^{-4}	0.40	0
10	810-880	6.5×10^{-5}	0.55	2200
11	880-920	8.6×10^{-6}	0.56	2760
12	920-1000	4.9×10^{-6}	0.54	2330
13	1000-1100	4.4×10^{-5}	0.52	2290
14	1100-1400	0	0.50	0
15	1400-2000	0	0.50	0
16	2000-2600	6.6	0.50	0
17	2600-8000	1.1×10^{-3}	0.50	0
18	1700-8000 (solar)	4.9×10^{-7}	0.27	0

Table 2

Pressure Scale Height in the Atmosphere of Venus as a Function of the CO_2 Concentration.

q(CO_2 per volume)	H_0 (cm)	q H_0 (cm)
1.0	5.901×10^5	5.901×10^5
0.75	6.491×10^5	4.865×10^5
0.5	7.212×10^5	3.606×10^5
0.25	8.114×10^5	2.029×10^5
0.1	8.771×10^5	8.771×10^4
0.05	9.015×10^5	4.508×10^4
0.01	9.210×10^5	9.210×10^3

For each spectral interval, the fractional absorption was computed from the expression

$$\bar{A}_i = 1 - e^{-\tau_i} , \tag{18}$$

where

$$\tau_i = (m_i u^*_i)^{n_i} . \tag{19}$$

The m_i are similar to the generalized absorption coefficients and the n_i are constants determined by the degree of overlapping of the individual lines and the slope of the curve of growth.

Wherever possible, the spectral intervals were chosen to coincide with the intervals used by Burch et al (Reference 13). The coefficients m_i and n_i were determined graphically by a fit of the strong line curve with applicable data points taken from this source. Where experimental data were not available the calculated tables of CO_2 absorption compiled by Stull et al. (Reference 14) were used. A sample is shown in Figure 2 and the various values of m and n are listed in Table 1.

The application of the strong line approximation is valid whenever the central regions of the various lines become opaque. For each spectral interval a check of the validity of the strong line

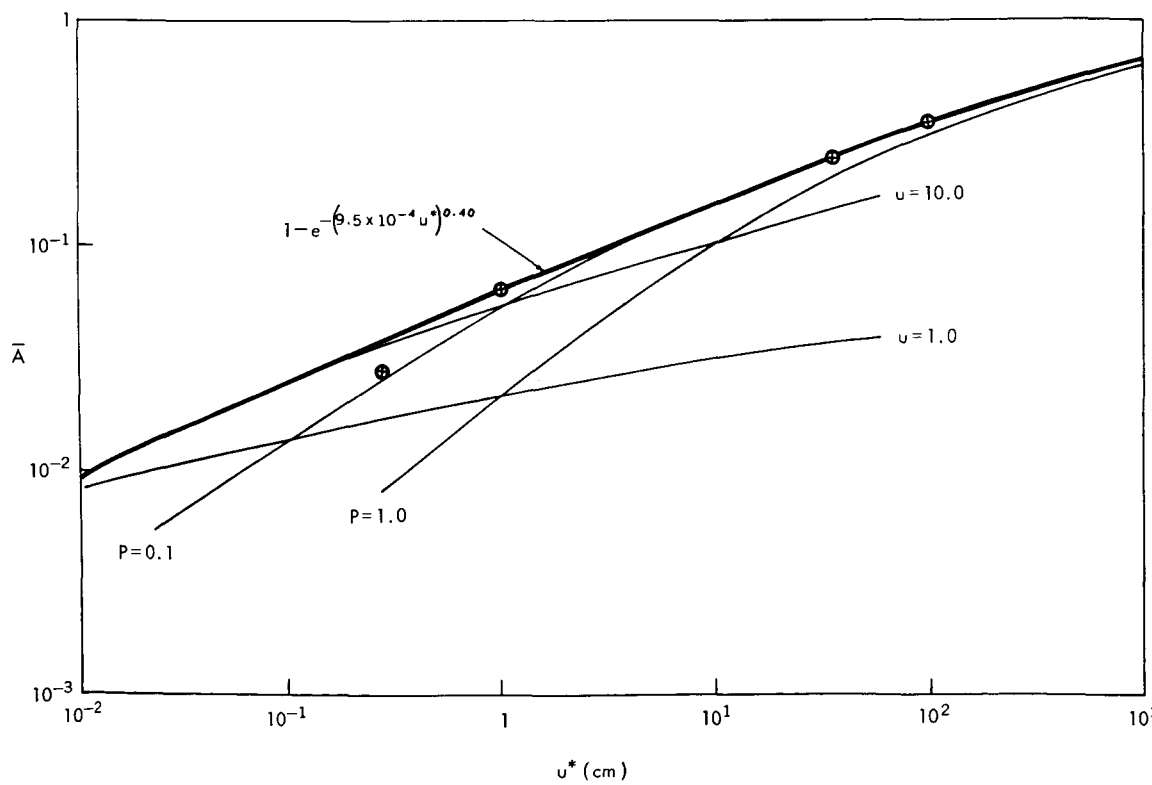

Figure 2—Illustration of strong line approximation fit for the spectral interval 720-810 cm^{-1}, as derived from Stull et al. (Reference 14). Data points taken from Burch et al. (Reference 13) and slightly modified are included for comparison.

approximation for the conditions considered was carried out. A relatively weak absorbing region (720-810 cm^{-1}) of the 15μ CO_2 band may serve as an illustration. If the approximation holds for this spectral interval, then it will be valid for stronger absorbing regions. According to Plass (Reference 7) the strong line approximation applies for all values of β to an accuracy of 10 percent, if $X > 1.63$. For this interval

$$\left.\begin{aligned} \beta &= 0.023\ P\ , \\ X &= 0.01\ \frac{u}{P}\ . \end{aligned}\right\} \qquad (20)$$

According to Equations 12 and 14, u/P equals qH_0 and defines the CO_2 concentration (see Table 2). As can be seen, the strong line approximation is valid within an accuracy of 10 percent for CO_2 concentrations in excess of 10^{-3} and more accurate for concentrations in excess of 10^{-2}, which is the range of interest for Venus.

SPECIFIC INTENSITY

The formulas derived in the section concerned with the solution of the radiative transfer equation must be expressed in terms of the adopted coordinate system. The specific intensity is a function of ν, τ, and μ and is conveniently expressed by upward and downward vectors. As mentioned before, the solution of the transfer equation appropriate here requires four components for the upward intensity:

1. Thermal emission from the cloud surface
2. Direct thermal emission from the atmosphere below interface j
3. Downward thermal emission from the whole atmosphere, reflected upward by the clouds
4. Downward solar radiation reflected upward by the clouds.

The downward intensity includes values for:

5. Direct emission from the atmosphere above interface j
6. Direct solar radiation.

These six components are shown in Figure 3 and discussed below.

Surface Emission

For a frequency interval i and an interface j, the thermal radiation emitted, which is attenuated between the surface and the interface j, is given by

$$I_{ij} = \epsilon_{ic} B_{ic} e^{-\frac{\tau_{ic} - \tau_{ij}}{\mu^n}} . \qquad (21)$$

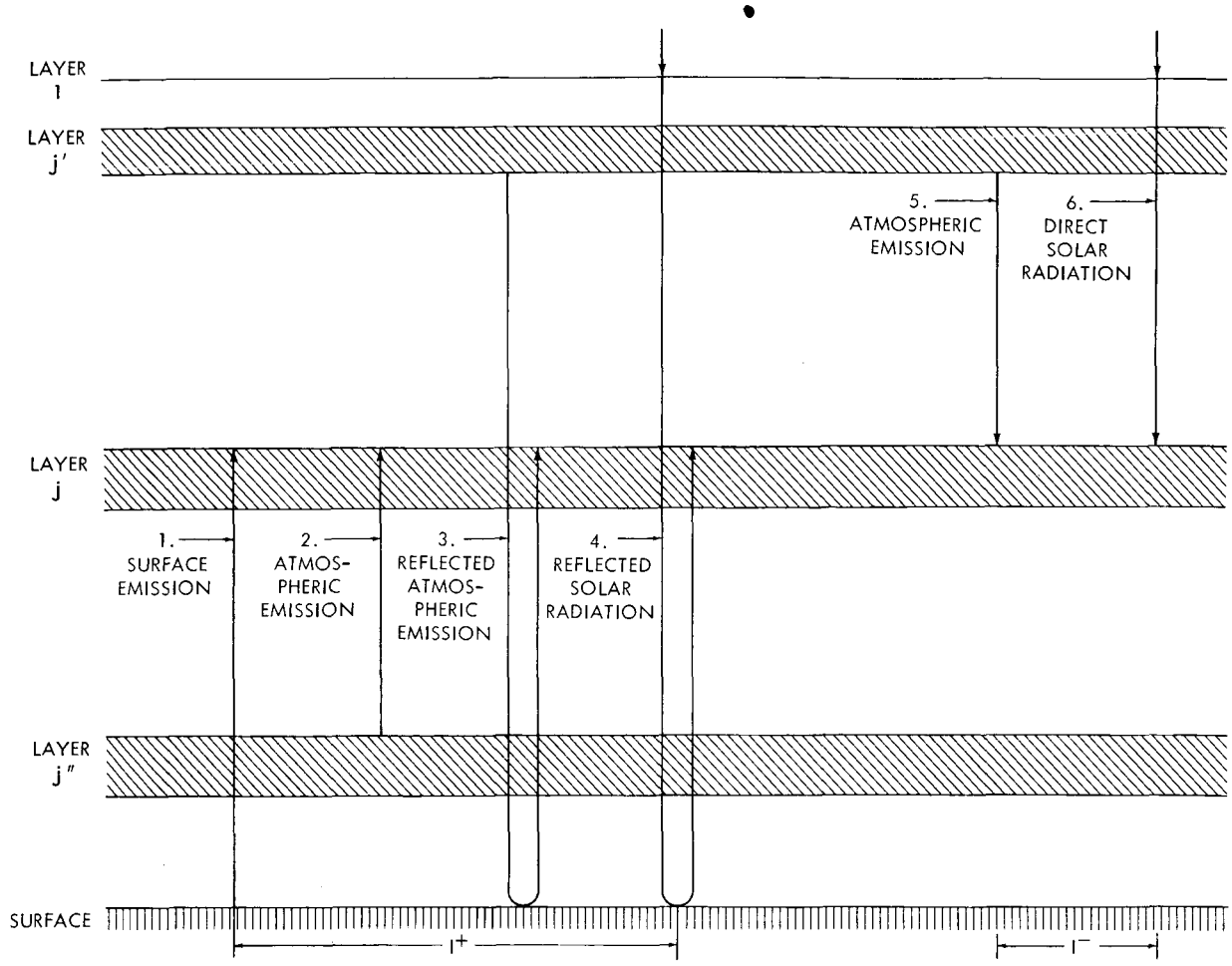

Figure 3–Schematic diagram of the radiation components considered.

The designation of emissivity applies directly for a solid or liquid surface, but some qualifications regarding the interpretation of ϵ_{ic} are necessary for a scattering medium such as a cloud surface. At this level the gas and cloud particles have a temperature T_c. For those spectral intervals where the atmospheric gas is opaque, the optical properties of the cloud particles are not important. In regions of the spectrum where the gas between particles is transparent the optical properties of the particles and their concentration become very important. For these intervals ϵ_c is defined as a boundary value, which indicates how much smaller the emerging radiation is compared with a blackbody at temperature T_c. The cloud emissivity was taken as unity in the strong absorption bands and set equal to a constant value in the transparent regions. In general, ϵ_{ic} may be a complicated function of wavelength and μ but this dependence is ignored.

Emission from the Atmosphere below Interface j

The contribution from each layer is proportional to the Planck function, an attenuation factor, and the optical thickness,

$$I_{ij} = \sum_{j'=j}^{33} B_{ij'} \, e^{-\frac{\tau_{ij'} - \tau_{ij}}{\mu^n}} \, \frac{\Delta\tau_{ij'}}{\mu^n} \quad . \tag{22}$$

Emission from the Atmosphere Reflected by the Clouds

This component is the product of the downward flux at the cloud surface, the reflectivity, and the attenuation factor of the atmosphere between the surface and τ_j. Since constant temperature is assumed within a layer, the flux integral (see below) can be integrated for each layer by using the recursion formula for exponential integrals,

$$E_n(\tau) \, d\tau = dE_{n+1}(\tau) \quad . \tag{23}$$

The reflected intensity becomes

$$I_{ij} = r_{ic} \, e^{-\frac{\tau_{ic} - \tau_{ij}}{\mu^n}} \, \frac{2}{n} \sum_{j'=1}^{33} B_{ij'} \left[E_{\frac{2}{n}+1}\left(\tau_{ic} - \tau_{i,\,j'+1}\right) - E_{\frac{2}{n}+1}\left(\tau_{ic} - \tau_{ij'}\right) \right] \quad . \tag{24}$$

Reflected Solar Radiation

Similarly, the reflected solar intensity is calculated from

$$I_{18,\,j} = \frac{S}{\pi} \, \zeta \, r_{18,\,c} \, e^{-\left(\frac{\tau_c}{\zeta^n} + \frac{\tau_c - \tau_j}{\mu^n}\right)} \quad . \tag{25}$$

Within the spectral range of 1.25 to 5.9μ the reflectivity of the clouds for solar radiation was taken equal to 0.6 which is consistent with recent observations (Reference 19). Again clouds were considered to be perfect diffusers.

Direct Emission from Atmospheric Layers above Interface j

This contribution is analogous to the emission from lower layers:

$$I_{ij} = \sum_{j'=1}^{j-1} B_{ij'} \, e^{-\frac{\tau_{ij} - \tau_{ij'}}{\mu^n}} \, \frac{\Delta\tau_{ij'}}{\mu^n} \quad . \tag{26}$$

Direct Solar Radiation

The direct solar radiation is given by the solar constant for 1.25 to 5.9μ appropriate for the distance of Venus (0.047 watt cm^{-2}):

$$I_{18,j} = \frac{S}{\pi} \zeta \, e^{-\frac{\tau_j}{\zeta^n}} \quad . \tag{27}$$

FLUX

The flux is derived conventionally by integration of the components of specific intensity over μ (Reference 9, for example):

$$\pi F = \int I \, \mu \, d\omega = 2\pi \int I \, \mu \, d\mu \quad . \tag{28}$$

Integration leads to exponential integrals of the form of

$$\int_0^1 e^{-\frac{\tau}{\mu^n}} \, \mu \, d\mu = \frac{1}{n} E_{\frac{2}{n}+1}(\tau) \quad , \tag{29}$$

$$\int_0^1 e^{-\frac{\tau}{\mu^n}} \frac{d\mu}{\mu^{n-1}} = \frac{1}{n} E_{\frac{2}{n}}(\tau) \quad . \tag{30}$$

The results are expressed by exponential integrals tabulated for integral order numbers (Reference 20). For all wavelength intervals concerned with thermal radiation ($i = 1$ to 17) n is close to 1/2; for integration, n was taken equal to 1/2, which leads to exponential integrals of the fifth and fourth orders respectively. For the interval concerned with solar radiation ($i = 18$) the exponent n is 0.27; for integration, n was taken equal to 1/4, which leads in this case to exponential integrals of the ninth and eighth orders respectively.

Analogous to the intensity, the upward flux consists of four components, and the downward flux consists of two.

The individual components of the upward flux F_{ij}^{+} are

1. $$4\epsilon_{ic} B_{ic} E_5(\tau_{ic} - \tau_{ij}) \quad , \tag{31}$$

2. $$4 \sum_{j'=j}^{33} B_{ij'} \left[E_5(\tau_{ij'} - \tau_{ij}) - E_5(\tau_{i,j'+1} - \tau_{ij}) \right] \quad , \tag{32}$$

3. $$16 r_{ic} E_5(\tau_{ic} - \tau_{ij}) \sum_{j'=1}^{33} B_{ij'} \left[E_5(\tau_{ic} - \tau_{i,j'+1}) - E_5(\tau_{ic} - \tau_{ij'}) \right] \quad , \tag{33}$$

4. $$8\frac{S}{\pi} r_{18,c}\, \zeta\, e^{-\frac{\tau_c}{\zeta^n}}\, E_9(\tau_c - \tau_j) \quad . \tag{34}$$

The components for the downward flux F_{ij}^- are

5. $$4\sum_{j'=1}^{j-1} B_{ij'}\left[E_5(\tau_{ij} - \tau_{i,j'+1}) - E_5(\tau_{ij} - \tau_{ij'})\right] \quad , \tag{35}$$

6. $$\frac{S}{\pi}\, \zeta\, e^{-\frac{\tau_j}{\zeta^n}} \quad . \tag{36}$$

The net flux $(\pi F_\nu = \pi F_\nu^+ - \pi F_\nu^-)$ is calculated for each layer j, for each wavelength interval i, and for the sum over all spectral intervals.

CONDITION OF RADIATIVE EQUILIBRIUM

The general condition of radiative equilibrium (Equation 8) will now be applied to an atmosphere consisting of many layers of finite optical thickness. For an element of area dA in a layer of optical thickness $\Delta\tau_\nu$, the element of reduced volume is

$$dV = \mu\, dA \left(\frac{\Delta u^*}{\mu}\right)^n \quad . \tag{37}$$

In this expression $\mu\, dA$ represents the projection of the element of area in a direction μ, and $(\Delta u^*/\mu)$ is the effective element of the radiating gas. For convenience and consistency with the equation for τ (Equation 2), l_ν in Equation 8 may be included with Δu^*. Upon inserting Equation 37 into Equation 8, the factor $(m\Delta u^*/\mu)^n\, e^{-\Delta\tau/\mu^n}$ becomes just the increment of absorptance of the layer. Upon integration from 0 to $\Delta\tau$ the radiative equilibrium condition becomes

$$\int_\nu \int_\mu I_\nu(\mu)\left(1 - e^{-\frac{\Delta\tau}{\mu^n}}\right)\mu\, d\mu\, d\nu = \int_\nu B_\nu \int_\mu \left(1 - e^{-\frac{\Delta\tau}{\mu^n}}\right)\mu\, d\mu\, d\nu \quad . \tag{38}$$

The computed intensities were inserted into Equation 38 and integration over μ was carried out analytically. In terms of the adopted coordinate system, the radiative equilibrium condition is

$$4\sum_{i=1}^{17}\epsilon_{ic}B_{ic}\left[E_5(\tau_{ic}-\tau_{i,j+1})-E_5(\tau_{ic}-\tau_{ij})\right]$$

$$+4\sum_{i=1}^{17}\sum_{\substack{j'=1\\ j'\neq j}}^{33}B_{ij'}\left[E_5\left(|\tau_{ij}-\tau_{i,j'+1}|\right)-E_5\left(|\tau_{i,j+1}-\tau_{i,j'+1}|\right)+E_5\left(|\tau_{i,j+1}-\tau_{ij'}|\right)-E_5\left(|\tau_{ij}-\tau_{ij'}|\right)\right]$$

$$+16\sum_{i=1}^{17}r_{ic}\left[E_5(\tau_{ic}-\tau_{i,j+1})-E_5(\tau_{ic}-\tau_{ij})\right]\sum_{j'=1}^{33}B_{ij'}\left[E_5(\tau_{ic}-\tau_{i,j'+1})-E_5(\tau_{ic}-\tau_{ij'})\right]$$

$$+\frac{S}{\pi}\zeta\left\{e^{-\frac{\tau_{18,j}}{\zeta^{1/4}}}\left(1-e^{-\frac{\Delta\tau_{18,j}}{\zeta^{1/4}}}\right)+8e^{-\frac{\tau_{18,c}}{\zeta^{1/4}}}r_{18,c}\left[E_9(\tau_{18,c}-\tau_{18,j+1})-E_9(\tau_{18,c}-\tau_{18,j})\right]\right\}$$

$$=2\sum_{i=1}^{17}B_{ij}\left[1-4E_5(\Delta\tau_{ij})\right]\quad . \tag{39}$$

The terms on the left side are arranged in the adopted sequence; the contribution from the surface, then the contribution from the atmosphere (direct and reflected), and finally solar radiation, (direct and reflected).

Radiation from the atmospheric layers above and below layer j is combined into one expression by the use of absolute value signs in the arguments of the exponential integrals. The right side represents the emission from layer j and the left side represents radiation absorbed by layer j.

The numerical solution of Equation 39 was carried out on an IBM 7094 computer. For each layer j and temperature T (between 100 and 350°K) the i wave number intervals of the right side of Equation 39 were summed by using the appropriate value of $\Delta\tau_{ij}$. A functional relationship between the total thermal emission E_j from a layer at temperature T_j was tabulated. The thermal emission from a layer depends on the Planck function and the optical thickness; both are functions of the temperature. The optical thickness depends on temperature through u^* (Equation 16). With this set of E vs. T tables for each layer, the calculation of the temperature profile continued as follows.

First the energy absorbed by a layer j (left side of Equation 39) was computed from an estimate of the temperature profile. After the absorbed energy was obtained, the computer searched the previously computed table for a temperature for layer j which balanced Equation 39. In other words, it determined the temperature at which layer j could reradiate the absorbed energy. This was repeated for each layer and the resulting temperature distribution was checked for constancy of the net flux. If the flux criterion was not satisfied, the computed temperature distribution was re-inserted and the iteration procedure continued.

The convergence criterion used in terminating the calculation was

$$\left| \frac{F_{(\text{layer } 10)} - F_{(\text{layer } j)}}{F_{(\text{layer } 10)}} \right| \leq \alpha \quad , \tag{40}$$

where α was chosen according to the desired accuracy. In general α was taken equal to 0.005. Obviously, higher accuracy would require more iterations. Once the convergence criterion was satisfied, the limb function was calculated in the final step,

$$\frac{I_i^+(j = 1, \mu)}{I_i^+(j = 1, \mu = 1)} \quad . \tag{41}$$

The limb function was computed for each spectral interval i and for a range of specified μ, by using the computed equilibrium temperature distribution. This expression (41) includes all upward components of the specific intensity.

The iteration process converges rapidly for low surface pressures, where, for a particular layer, radiation from the surface dominates radiation from other atmospheric layers. For optically dense atmospheres the convergence process takes much longer. These effects are demonstrated in Figures 4 and 5 where samples of the iteration process for low and high surface pressures and for low and high initial temperature estimates are shown. More general studies of the convergence of iterative processes are available (Reference 21, for example).

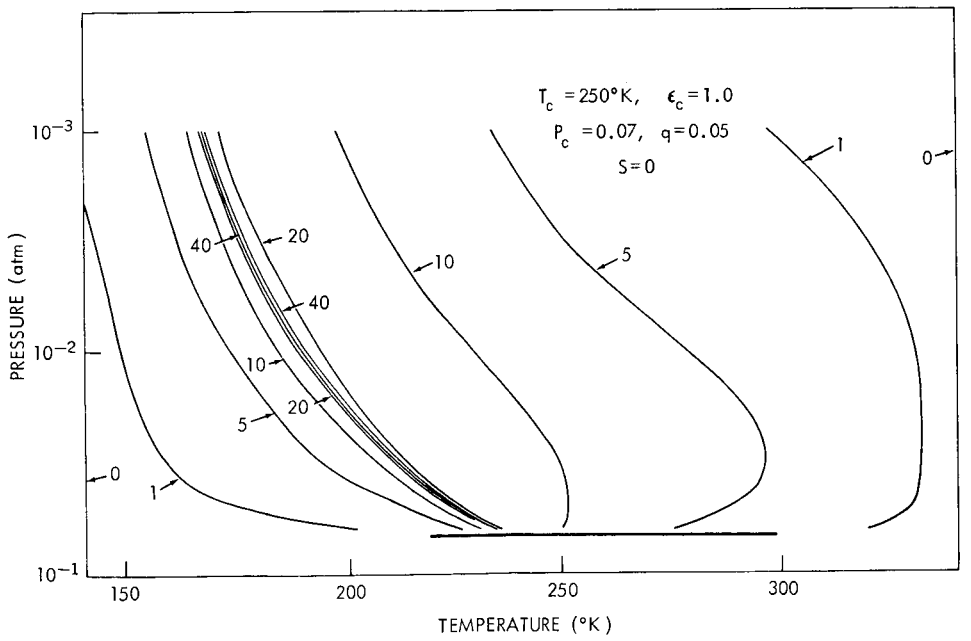

Figure 4—Sample of the convergence of the iteration process for an optically thin atmosphere. The numerals adjacent to each curve in the figure indicate the iteration number corresponding to each temperature distribution shown.

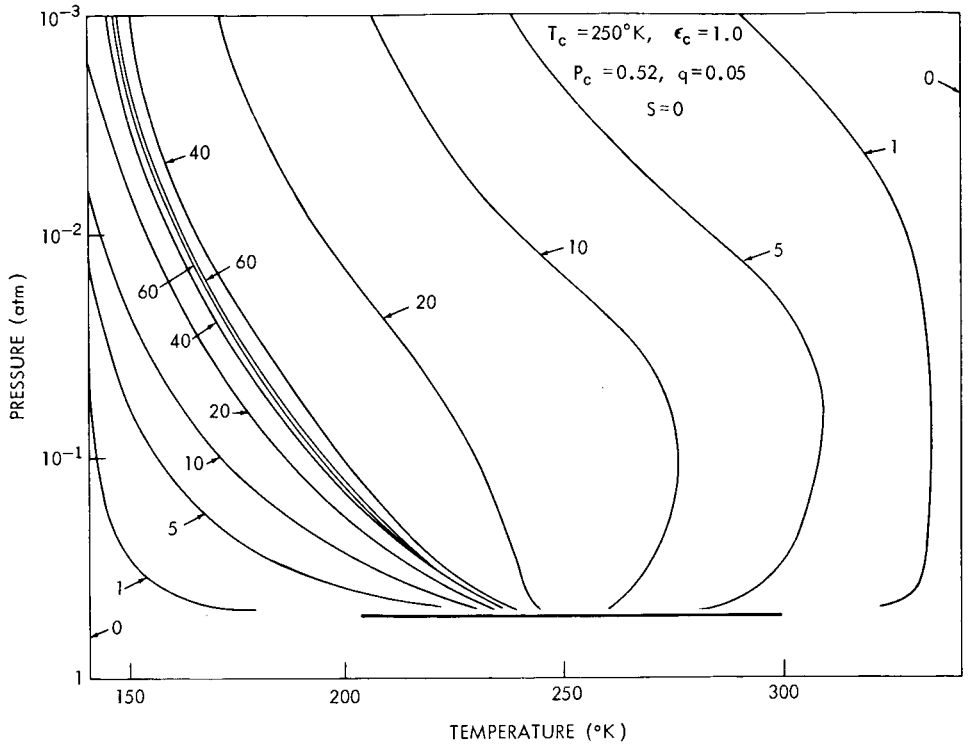

Figure 5—Sample of the convergence of the iteration process for a more optically dense atmosphere than that considered in Figure 4. The numerals adjacent to each curve in the figure indicate the iteration number corresponding to each temperature distribution shown.

RESULTS

As stated earlier, a portion of the atmosphere of Venus was selected for analysis with the formulated program. Several sets of good observational material presently exist which can serve as a basis for comparison with the computed results.

The atmosphere of Venus above the clouds is more amenable to analysis and consequently is better understood than the region between the surface and the upper cloud layer (References 22-27). However, starting from essentially the same set of observational data, various students of Venus have reached different conclusions. Estimates of the cloud top pressure range from 0.007 to 1 atm (References 23 and 28-30). Large discrepancies exist in estimates of the water vapor content (References 31-33), and the abundance of CO_2 (References 34-36) is still subject to discussion. The reasons for the discrepancies are many-fold, but the solution to the problem will depend on better observations and more refined interpretation of existing data.

The interpretation of the intensities measured within the atmospheric window by Sinton and Strong (Reference 16), Murray, Wildey and Westphal (Reference 17), and by Chase, Kaplan, and Neugebauer (Reference 18) clearly requires some knowledge of the temperature profile in the upper atmosphere of Venus. So far, only the black-transparent model used by Mintz (Reference 37) and

the grey model used by Rasool (Reference 38) and Ostriker (Reference 39) have been applied. None of these calculations consider the strong temperature dependence of the 9.4 and 10.4μ CO_2 excited bands or the solar heating in the clear atmosphere.

It is instructive to note that early application of the grey atmospheric model to the earth's atmosphere by Humphreys (Reference 40), Gold (Reference 41), and Emden (Reference 42) yielded only crude agreement between calculations and reality. Subsequent treatments (References 5 and 43-47, for example) which included the wavelength dependence of the H_2O, CO_2, and O_3 absorption were necessary for satisfactory temperature profiles. Similarly, a more exact and detailed study of the atmosphere of Venus should give better results.

Highly developed nongrey atmospheric models (Reference 48, for example) used to describe the earth's stratosphere exist but have not been applied to Venus. However, recent work by Arking (Reference 49) and Ohring (Reference 46) with nongrey models have been applied to the atmosphere of Mars. For Venus, the discrepancies in estimates of composition, cloud top pressure, and other parameters necessary for accurate calculations have probably discouraged the application of these models. Furthermore, CO_2 absorption coefficients for relatively large concentrations have become available only recently (References 13, 14, and 50). However, it is felt that a parametric study with a variety of values for cloud top pressure and temperature and for CO_2 concentration should improve our understanding of the physical conditions in the atmosphere of Venus. Results of the calculations can be compared with existing and forthcoming measurements, and the range of values for important parameters then, hopefully, can be narrowed.

The effect of solar heating, carbon dioxide concentration, and assumed cloud top pressure, temperature, and emissivity, on the atmospheric temperature above the clouds can now be discussed. A number of conclusions can be drawn from this parametric study. However, the attempt to match, in detail, the calculated intensities, fluxes, and limb functions with the observations is still underway.

The pronounced effect of solar heating in the clear atmosphere is apparent in Figure 6. A realistic interpretation of planetary observations of a partially illuminated disk requires further averaging over zenith angles. The temperature maximum disappears for larger zenith angles and the temperature distribution approaches the equilibrium condition on the dark side. Three factors make the large amount of solar heating understandable. Relative to the earth, the solar constant is nearly double; secondly, the high reflectivity of the clouds gives rise to strong reflected radiation and consequently to an additional heat source; and finally, the CO_2 concentration

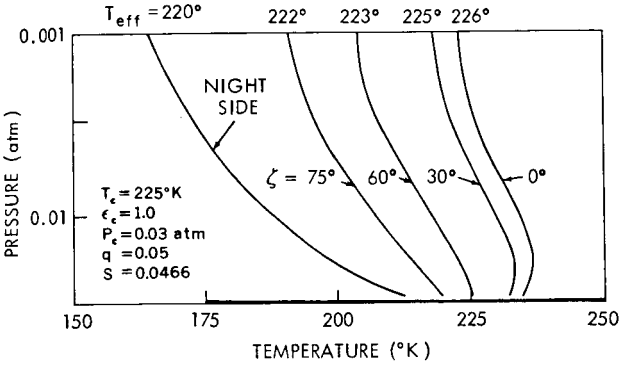

Figure 6—Radiative equilibrium temperature distribution in the Venus atmosphere, illustrating the effects of solar heating for various solar zenith angles.

is much higher. The high CO_2 concentration increases the ability of the layers to cool very effectively, but at long wavelengths many spectral regions are already saturated. This atmospheric greenhouse effect is very pronounced. The near infrared absorption region considered in this discussion, spectral interval number 18 (1.25-5.9μ), would saturate at much higher pressures (between 3 and 10 atmospheres). Observations at the 8-12μ window and at 3.75μ (Reference 51) indicate essentially the same brightness temperatures in the sunlit and dark hemispheres. This is not in contradiction to the calculated large temperature differences in the clear atmosphere since the observations exist only for relatively transparent spectral regions. Larger differences are expected in moderately strong absorption regions, but unfortunately data are not available there.

The equilibrium temperatures with and without solar heating for various cloud top pressures are illustrated in Figure 7. For low cloud top pressures and consequently low optical thicknesses, the surface can be observed more readily and hence the effective temperature approaches the cloud top temperature. The discontinuity in the temperature profile near the lower boundary is characteristic of radiative equilibrium considerations in a bounded, finite atmosphere and has been discussed by several authors (References 5 and 52, for example). A more realistic representation of the cloud top which does not assume a "solid surface" will remove the discontinuity and limit the gradient to an adiabatic one. If necessary, allowance for convective as well as radiative transport of energy must be made. It can be also seen from Figure 7 that some of the calculated gradients approach and even exceed the adiabatic one near the cloud top surface. Convection would be induced and an upward transport of cloud particles would occur.

A curve which indicates saturation temperatures for CO_2 is included in Figure 7. For the conditions considered, condensation and possible formation of CO_2 clouds is unlikely. The wide spread and the slope of temperature profiles shown in Figure 7 make it difficult to extrapolate the temperatures, in detail, to much lower pressures. Caution must be exercised, especially in extrapolations to the low pressures for the occultation measurements $\approx 2.6 \times 10^{-6}$ atm (Reference 53).

The effects of CO_2 concentration on the temperature distribution (Figure 8) are different for the dark and sunlit hemispheres of the planet. On the dark side, the temperatures depend very little on the CO_2 concentration, with the exception of very high layers which can cool more effectively for the higher concentrations. The effects of solar heating have already been discussed.

The temperature distribution of a grey atmospheric model is included for comparison and clearly illustrates the difference between the isothermal character of the grey model and the larger gradients obtained by applying nongrey absorption.

The final illustration (Figure 9) demonstrates the effect of nonblackness for the cloud top surface. The total net flux is kept approximately the same for all cases by adjusting the surface temperature upwards as the emissivity is lowered. As discussed before, the value of ϵ was set equal to unity for the intervals $i = 7$, 8, and 16, where CO_2 absorption is strongest. In all other intervals ϵ was set equal to the value designated in the figure. The effect on the resulting temperature distribution is small.

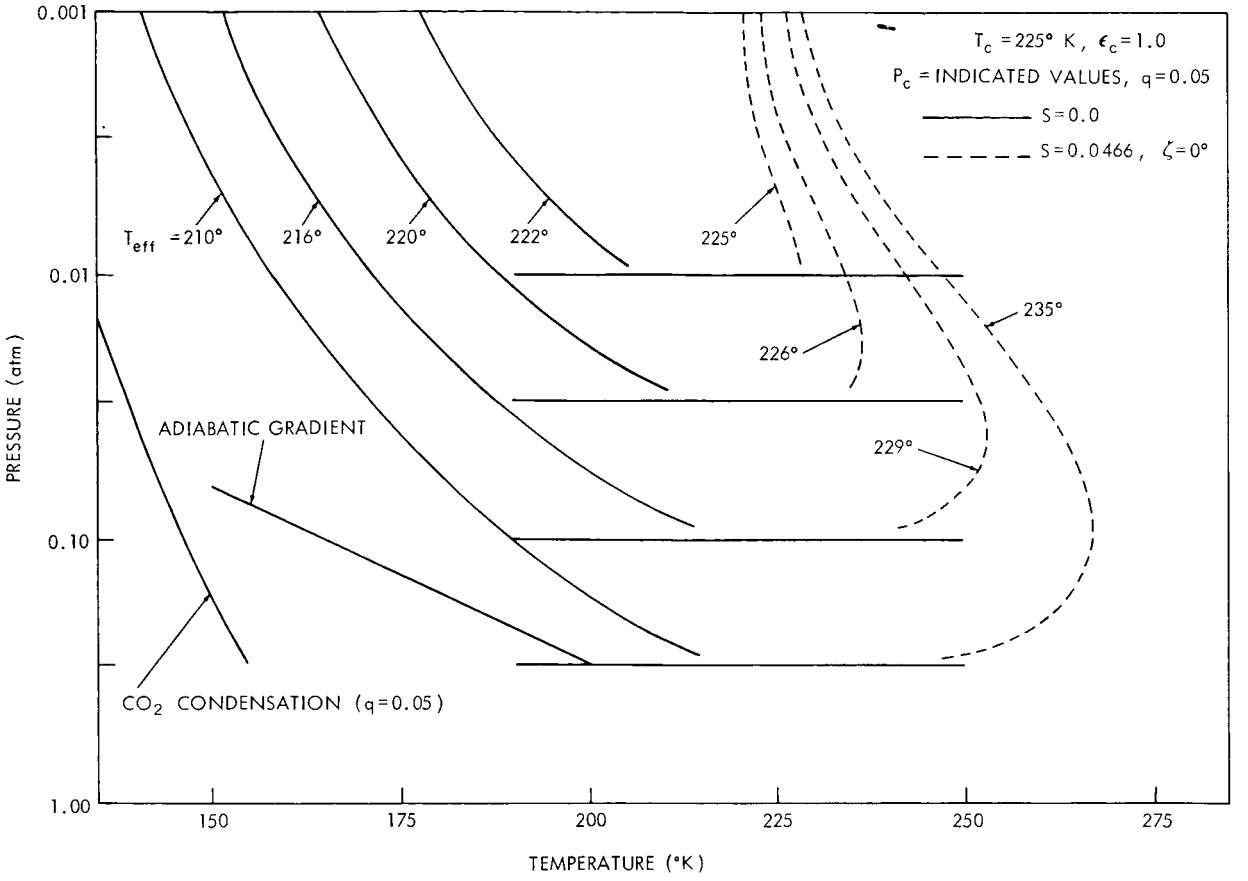

Figure 7–Radiative equilibrium temperature distributions as a function of cloud top pressure level, for the dark and sunlit hemispheres.

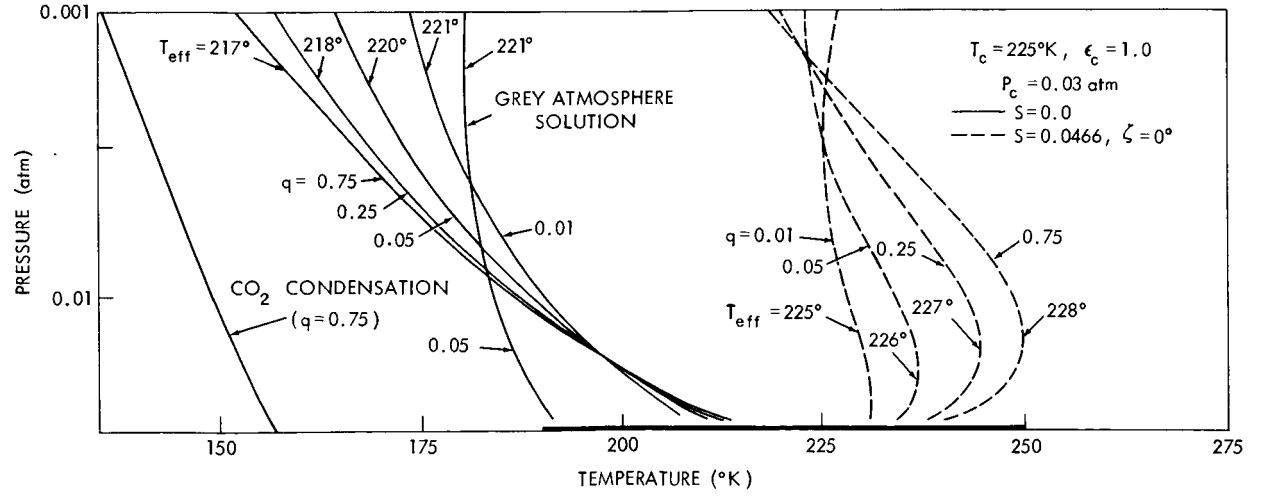

Figure 8–Radiative equilibrium temperature distributions showing the effects of various CO_2 concentrations, for the dark and sunlit hemispheres.

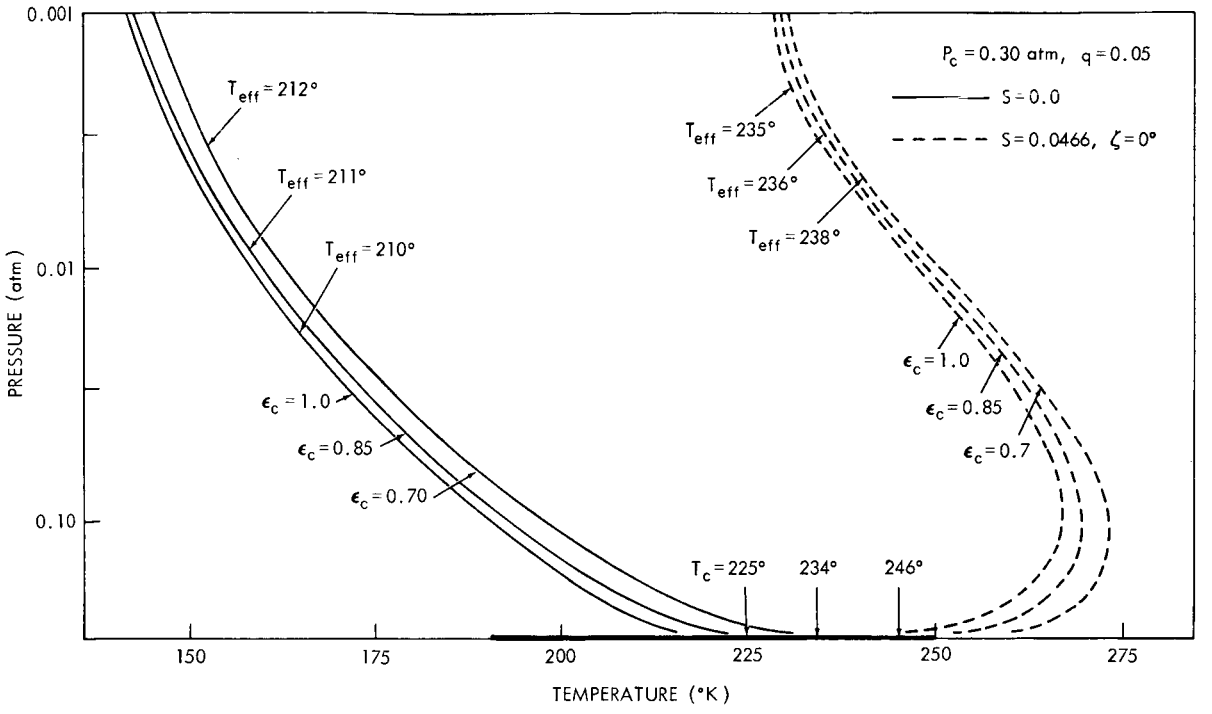

Figure 9—Radiative equilibrium temperature distributions illustrating the effect of cloud top emissivity and temperature, for an almost constant net flux, for the dark and sunlit hemispheres.

In summary then, radiative transfer calculations, which include pressure, temperature, and wavelength dependence of molecular absorption, are a strong analytical tool for the exploration of planetary atmospheres. The full capability of this tool has by far not been exhausted. Further analysis of the spectral and angular dependence of the emitted energy is required for more specific conclusions.

ACKNOWLEDGMENTS

The authors would like to express their gratitude to the following people for their contributions to the effort presented here: Mr. A. F. Simmons, for an expertly written computer program, Mr. T. Mahuron and Miss L. Coury for numerous calculations, and Mr. W. R. Bandeen and Dr. F. Möller for helpful criticism and discussion.

(Manuscript received February 25, 1964)

REFERENCES

1. Elsasser, W. M., and Culbertson, M. F., "Atmospheric Radiation Tables," *Meteorol. Monographs* 4(23):1-43, August 1960.

2. Kaplan, L. D., "On the Calculation of Atmospheric Transmission Functions for the Infrared," *J. Meteorol.* 9(2):139-144, April 1952.

3. Plass, G. N., "Parallel-Beam and Diffuse Radiation in the Atmosphere," *J. Meteorol.* 9(6):429-436, December 1952.

4. Kourganoff, V., "Basic Methods in Transfer Problems; Radiative Equilibrium and Neutron Diffusion," Oxford: Clarendon Press, 1952.

5. Goody, R. M., "The Thermal Equilibrium at the Tropopause and the Temperature of the Lower Stratosphere," *Roy. Soc. Proc.* Ser. A, 197(1051):487-505, July 7, 1949.

6. Chamberlain, J. W., and Kuiper, G. P., "Rotational Temperature and Phase Variation of the Carbon Dioxide Bands of Venus," *Astrophys. J.* 124(2):399-405, September 1956.

7. Plass, G. N., "Useful Representations for Measurements of Spectral Band Absorption," *J. Opt. Soc. Amer.* 50(9):868-875, September 1960.

8. Milne, E. A., "Thermodynamics of the Stars," *Handbuch der Astrophysik* 3(1):65-255, 1930.

9. Chandrasekhar, S., "Radiative Transfer," Oxford: Clarendon Press, 1950.

10. Goody, R. M., "Physics of the Stratosphere," Cambridge Univ. Press, 1958.

11. Plass, G. N., and Fivel, D. I., "Influence of Doppler Effect and Damping on Line-Absorption Coefficient and Atmospheric Radiation Transfer," *Astrophys. J.* 117(1):225-234, January 1953.

12. Strong, J., and Plass, G. N., "The Effect of Pressure Broadening of Spectral Lines on Atmospheric Temperature," *Astrophys. J.* 112:365-379, November 1950.

13. Burch, D. E., Gryvnak, D., and Williams, D., "Infrared Absorption by Carbon Dioxide," Ohio State University Research Foundation, Columbus, report SR-2, January 1961.

14. Stull, V. R., Wyatt, P. J., and Plass, G. N., "The Infrared Absorption of Carbon Dioxide," Air Force Systems Command, Los Angeles, California, report SSD-TDR-62-127, V. III, January 1963.

15. Yamamoto, G., "Direct Absorption of Solar Radiation by Atmospheric Water Vapor, Carbon Dioxide and Molecular Oxygen," *J. Atmos. Sci.* 19(2):182-188, March 1962.

16. Sinton, W. M., and Strong, J., "Radiometric Observations of Venus," *Astrophys. J.* 131(2):470-490, March 1960.

17. Murray, B. C., Wildey, R. L., and Westphal, J. A., "Infrared Photometric Mapping of Venus through the 8-14 Micron Atmosphere Window," *J. Geophys. Res.* 68(16):4813-4818, August 1963.

18. Chase, S. C., Kaplan, L. D., and Neugebauer, G., "The Mariner 2 Infrared Radiometer Experiment," *J. Geophys. Res.* 68(22):6157-6170, November 1963.

19. Moroz, V. I., "The Infrared Spectrum of Venus (1-2.5μ)," *Sov. Astronom. AJ* 7(1):109-115, July-August 1963.

20. Pagurova, V. I., "Tables of the Exponential Integral," London: Pergamon Press, 1961.

21. Stone, P. H., "Approximate Integral Equations for the Temperature in Non-Gray Model Atmospheres," *Astrophys. J.* 137(2):628-640, February 1963.

22. Urey, H. C., "The Atmospheres of the Planets," *in: Handbuch der Physik* (S. Elügge, ed.), V. 52:363-418, Berlin: Springer-Verlag, 1959.

23. Opik, E. J., "The Aeolosphere and Atmosphere of Venus," *J. Geophys. Res.* 66(9):2807-2819, September 1961.

24. Kuiper, G. P., "Planets and Satellites, V. 3, The Solar System," (Kuiper, G. P., and Middlehurst, B. M., ed.) Chicago: Univ. of Chicago Press, 1961.

25. Rea, D. G., "Molecular Spectroscopy of Planetary Atmospheres," *Space Sci. Rev.* 1(2):159-196, October 1962.

26. Sagan, C., and Kellogg, W. W., "The Terrestrial Planets," *Ann. Rev. Astron. Astrophys.* 1:235-266, 1963.

27. Rozenberg, G. V., "Investigations of the Atmosphere of the Planet Venus by Optical Methods," *Sov. Phys. Doklady,* 8(1):1-2, July 1963.

28. Kaplan, L. D., "A Preliminary Model of the Venus Atmosphere," Jet Propulsion Laboratory, California Institute of Technology, Pasadena, report JPL TR-32-379, December 12, 1962.

29. Sagan, C., "The Radiation Balance of Venus," California Institute of Technology, Pasadena, report JPL TR-32-34, September 15, 1960.

30. Anderson, C. E., and Evans, D. C., "The Nature of the Venus Cloud System," Institute of Aerospace Science paper, National Summer Meeting, Los Angeles, California, June 18-22, 1962.

31. Strong, J., Ross, M. D., and Moore, C. B., "Some Observations on the Atmosphere of Venus and the Earth during the Strato Lab IV Balloon Flight," *J. Geophys. Res.* 65(8):2526, August 1960.

32. Spinrad, H., "A Search for Water Vapor and Trace Constituents in the Venus Atmosphere," *Icarus* 1(3):266-270, October 1962.

33. Dollfus, A., "Observations of Water Vapor on the Planet Venus," *C. R. Acad. Sci.* 256(15):3250-3253, April 8, 1963 (In French).

34. Dunham, T., Jr., "Spectroscopic Observations of the Planets at Mount Wilson," in: "The Atmospheres of the Earth and Planets," (G. P. Kuiper, ed.) 288-305, Chicago: Univ. of Chicago Press, 1952, pp 288-305.

35. Kaplan, L. D., "A New Interpretation of the Structure and CO_2 Content of the Venus Atmosphere," *Planet. Space Sci.* 8(1):23-29, October 1961.

36. Spinrad, H., "Spectroscopic Temperature and Pressure Measurements in the Venus Atmosphere," *Astron. Soc. Pacific Publ.* 74:187-201, June 1962.

37. Mintz, Y., "Temperature and Circulation of the Venus Atmosphere," *Planet. Space Sci.* 5(2):141 152, June 1961.

38. Rasool, S. I., "Structure of Planetary Atmospheres," *AIAA J.* 1(1):6-19, January 1963.

39. Ostriker, J. P., "Radiative Transfer in a Finite Gray Atmosphere," *Astrophys. J.* 138(1):281-290, July 1963.

40. Humphreys, W. J., "Vertical Temperature-Gradients of the Atmosphere, Especially in the Region of the Upper Inversion," *Astrophys. J.* 29:14-32, January 1909.

41. Gold, E., "The Isothermal Layer of the Atmosphere and Atmospheric Radiation," *Roy. Soc. Proc.* Ser. A, 82(551):43-70, February 1909.

42. Emden, R., "Über Strahlungsgleichgewicht und Atmosphärische Strahlung. Ein Beitrag zur Theorie der Oberen Inversion," *Sitzungsberichte der mathematisch-physikalischen Klasse,* Akademie der Wissenschaften, Munchen, Part I: 55-142, January-March 1913.

43. Simpson, G. C., "Studies in Terrestrial Radiation," *Roy. Meteorol. Soc. Mem.* 2(16):69-95, March 1928.

44. King, J. I. F., "Line Absorption and Radiative Equilibrium," *J. Meteorol.* 9(5):311-321, October 1952.

45. Yamamoto, G., "Radiative Equilibrium of the Earth's Atmosphere, I. The Grey Case," *Science Reports of the Tohoku University, 5th Series, Geophysics* 5(2):45-57, October 1953.

46. Ohring, G., "A Theoretical Estimate of the Average Vertical Distribution of Temperature in the Martian Atmosphere," *Icarus,* 1(4):328-333, January 1963.

47. Kondrati'ev, K., "Teplovoi Rezhim Verkhnikh Sloev Atmosfery," ("Thermal Conditions of Upper Strata of the Atmosphere"). Leningrad: Gidrometeoizdat, 1960.

48. Manabe, S., and Möller, F., "On the Radiative Equilibrium and Heat Balance of the Atmosphere," *Monthly Weather Rev.* 89(12):503-532, December 1961.

49. Arking, A., "Non-Grey Convective Planetary Atmospheres," Eleventh International Astrophysical Symposium, Liege, July 9-12, 1962, 7:180-189, 1963.

50. Howard, J. N., Burch, D. E., and Williams, D. E., "Near-infrared Transmission Through Synthetic Atmospheres," Ohio State University Research Foundation, Columbus, report SR-1, December 1954.

51. Sinton, W. M., *Proc. Eleventh Internat. Astrophys. Sym.,* Liege, July 9-12, 1962.

52. Möller, F., "Über das Strahlungsgleichgewicht in der Nähe der Erdoberfläche," *Meteorol Runds.* 13(5):134-139, September-October 1960.

53. Menzel, D. H., and de Vaucouleurs, G., "Final Report on the Occultation of Regulus by Venus, July 7, 1959," Harvard College Observatory, Cambridge, report SR-1, January 10, 1961.